Multiphoton ionization of xenon in the vuv regime

Robin Santra and Chris H. Greene

Department of Physics and JILA, University of Colorado, Boulder, Colorado 80309-0440, USA

(Received 2 July 2004; published 3 November 2004)

In a recent experiment at the vuv free-electron laser facility at DESY in Hamburg, the generation of multiply charged ions in a gas of atomic xenon was observed. This paper develops a theoretical description of the multiphoton ionization of xenon and its ions. The numerical results lend support to the view that the experimental observation may be interpreted in terms of the nonlinear absorption of several vuv photons. The method rests on the Hartree-Fock-Slater independent-particle model. The multiphoton physics is treated within a Floquet scheme. The continuum problem of the photoelectron is solved using a complex absorbing potential. Rate equations for the ionic populations are integrated to take into account the temporal structure of the individual vuv laser pulses. The effect of the spatial profile of the free-electron laser beam on the distribution of xenon charge states is included. An Auger-type many-electron mechanism may play a role in the vuv multiphoton ionization of xenon ions.

I. INTRODUCTION

An electron bound to an atom experiences electric forces, which on average point toward the atomic nucleus. If the atom is placed in a static electric field, the electronic states become unstable, as the potential arising from the superposition of the atomic and the external electric field enables electron emission via tunneling. This picture basically remains valid even if the external electric field is oscillating, at least as long as the oscillation period of the electric field is long in comparison to the electron tunneling time scale [1–5]. For a typical valence-electron binding energy of the order of 10 eV and a laser photon energy of about 1 eV—i.e., in the ir regime—the tunneling picture is meaningful for intensities of 10^{13} W/cm^2 or higher. However, at high radiation frequency (or at low intensity), this picture fails, and it is more appropriate to adopt a multiphoton picture [6–9]: An atomic electron can be ejected following the absorption of a discrete number of photons.

The development of free-electron laser (FEL) [10] facilities at several places in the world [11] has spurred substantial theoretical interest [12–21], but until very recently, no radiation sources have been available to experimentally probe strong-field physics at vuv or shorter wavelengths. The situation changed when the VUV-FEL at DESY, Hamburg, began operation [22,23]. In one of the first experiments with this exceptional radiation source, xenon clusters were exposed to intense vuv laser pulses and were observed to absorb a surprisingly large number of vuv photons per atom [24], a finding which was explained in terms of inverse bremsstrahlung [25]. No evidence for atomic multiphoton processes was found in these first measurements. Measurements using a more sensitive detector, however, revealed the creation of multiply charged ions even in a gas of free, unclustered xenon atoms [26]. An experimental time-of-flight mass spectrum, averaged over 100 consecutive VUV-FEL pulses, is shown in Fig. 1 [27]. The photon energy in that experiment was 12.7 eV with a peak intensity of approximately 10^{13} W/cm^2.

In this paper, we present a theoretical description of the interaction of xenon atoms with an intense pulse of vuv photons. Our findings lend support to the interpretation that the occurrence of multiply charged ions, as reported in Ref. [26], is a consequence of vuv multiphoton ionization—a scientific first at a photon energy of more than 10 eV. We describe our computational method in Sec. II. In Sec. III, the results of our calculations are presented and compared with experiment. We conclude with Sec. IV. Atomic units are used throughout, unless otherwise noted.

II. COMPUTATIONAL METHOD

Using an independent-electron model, Geltman [28] (see also Refs. [29,30]) was able to arrive at a satisfactory representation of the ionic charge distributions observed in several intense-laser experiments at photon energies of 6.4 eV and
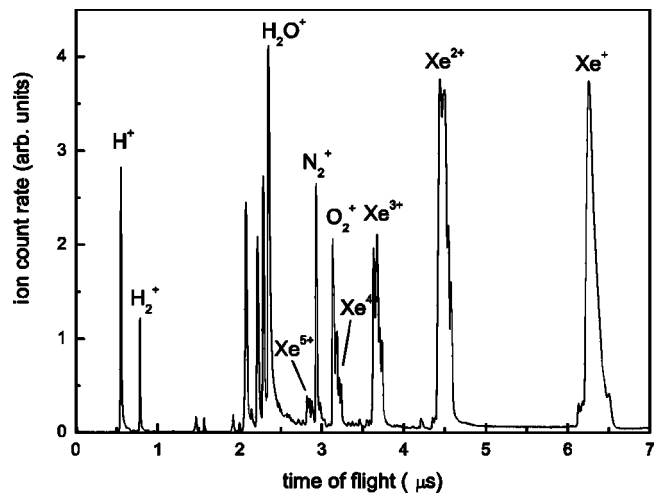

FIG. 1. Experimental [27] ion detection signal is plotted versus the ionic time of flight. Free-electron laser pulses with a peak intensity of about 10^{13} W/cm^2, a duration of approximately 100 fs, and a photon energy of 12.7 eV produce, in an atomic xenon beam, ionic species of various charge states [26]. This time-of-flight mass spectrum [27] is an average over 100 consecutive FEL pulses.

TABLE I. $X\alpha$ parameters employed to reproduce the $5p$ ionization potential (I.P.) of Xe^{q+}—i.e., the energy needed to remove one electron from Xe^{q+} and generate $Xe^{(q+1)+}$ in its ground state. Also shown is the minimum number of 12.7-eV photons (N.P.) needed to ionize Xe^{q+}.

q	I.P. [eV]	$X\alpha$	N.P.
0	12.1[a]	1.067	1
1	21.0[b]	1.031	2
2	31.1[c]	1.180	3
3	42[d]	1.056	4
4	53[e]	1.044	5
5	64[f]	0.999	6

[a]Reference 41.
[b]Reference 42.
[c]Reference 43.
[d]Reference 44.
[e]Reference 45.
[f]Reference 47.

below [31–35]. Within the framework of independent particles, each electron moves in the field of the atomic nucleus and in a mean field generated by the other electrons. The best such mean field derives from the Hartree-Fock self-consistent-field method [36]. However, the Hartree-Fock mean field is nonlocal, due to the exchange interaction, and therefore cumbersome to work with. Slater [37] introduced a local approximation to electron exchange, which is the principle underlying the well-known $X\alpha$ method [38].

In this work, we use the Hartree-Fock-Slater code written by Herman and Skillman [39], which in the past has proved advantageous for atomic photoionization studies (see, for example, Ref. [40]). The resulting one-electron potential $V_{HS}(r)$ is a central potential (even for open-shell systems), which satisfies

$$V_{HS}(r) \rightarrow -Z/r, \quad r \rightarrow 0, \tag{1}$$

$$V_{HS}(r) \rightarrow -(q+1)/r, \quad r \rightarrow \infty, \tag{2}$$

for an atom of nuclear charge $+Z$ and overall charge $+q$. In the original program of Herman and Skillman, the $X\alpha$ parameter was set to unity, in accordance with Ref. [37]. We adjusted that parameter slightly (see Table I), so that the calculated $5p$ binding energy in Xe, Xe^+, Xe^{2+}, and Xe^{3+} agrees with experimental data [41–44]. The situation is a little more complex for Xe^{4+} and Xe^{5+}. The experimental ionization potentials of these ions, as determined from measured electron-impact ionization thresholds [45–47], vary by as much as 18 eV. Utilizing the complete-active-space self-consistent-field (CASSCF) code implemented in the *ab initio* program package MOLPRO [48,49], an active space consisting of the $4d$, $5s$, $5p$, $6s$, and $6p$ orbitals, and an effective core potential [50], we obtained ionization potentials of 53 and 64 eV for Xe^{4+} and Xe^{5+}, respectively. The value for Xe^{4+} agrees with Ref. [45]; the one for Xe^{5+} is in agreement with Ref. [47]. As indicated in Table I, we base the $X\alpha$ parameters for Xe^{4+} and Xe^{5+} on the ionization potentials quoted above.

It should be mentioned that while our CASSCF calculation includes scalar relativistic effects in an approximate manner (through the effective core potential), spin-orbit splittings have not been taken into account.

We represent the radial one-electron Hamiltonian

$$H_{AT}^{(l)} = -\frac{1}{2}\frac{d^2}{dr^2} + \frac{l(l+1)}{2r^2} + V_{HS}(r) \tag{3}$$

in a finite-element basis set [51–56], which is described in detail in Ref. [57]. In the calculations reported here, 4801 finite-element basis functions were employed, spanning a radial grid from $r_{min}=0$ to $r_{max}=80$ Bohr radii. For each orbital angular momentum quantum number l considered, the first 50 eigenfunctions $u_{n,l}(r)$ of $H_{AT}^{(l)}$ were computed that have eigenenergies $\varepsilon_{n,l}$ at least as high as the energy $\varepsilon_{5,0}$ of the $5s$ level. More strongly bound levels are assumed to be fully occupied by core electrons and are not considered any further. The calculated eigenfunctions $u_{n,l}(r)$ satisfy the boundary conditions $u_{n,l}(r_{min})=0$ and $u_{n,l}(r_{max})=0$. At the current level of approximation, atomic multiplet structure is absent. All electrons that can be associated with the quantum numbers n and l have the same energy $\varepsilon_{n,l}$ within our model. In particular, there is no energy dependence on the magnetic quantum number m.

In order to treat the problem of electron emission, a complex absorbing potential (CAP) [58–74] $-i\eta W(r)$ is added to the atomic Hamiltonian. The real, positive parameter η is the CAP strength. The local one-electron potential $W(r)$ is chosen here as

$$W(r) = \begin{cases} 0, & 0 \leq r < c, \\ (r-c)^2, & r \geq c, \end{cases} \tag{4}$$

where $c=4$ a.u. in this paper (which places the absorbing potential right outside the ionic core). The CAP absorbs the outgoing electron and renders the associated wave function square integrable. Given a complete basis, there exists for a resonance eigenstate (a Gamow vector) of the physical Hamiltonian with Siegert eigenvalue $E_{res}=E_R-i\Gamma/2$, an eigenvalue $E(\eta)$ of the CAP-augmented Hamiltonian such that $\lim_{\eta\rightarrow0^+} E(\eta)=E_{res}$ [62]. In a finite basis set, η_{opt} must be found, satisfying [62]

$$\left| \eta \frac{dE(\eta)}{d\eta} \right|_{\eta_{opt}} = \text{minimum}. \tag{5}$$

$E(\eta_{opt})$ provides an approximation to the Siegert energy E_{res}, from which the resonance position E_R and the resonance width Γ can be extracted. An improved strategy, which is used here, consists in analyzing the function $E(\eta)$ $-\eta dE(\eta)/d\eta$ and minimizing $|\eta^2 d^2 E(\eta)/d\eta^2|$ [62].

Within the framework of quantum electrodynamics [75], the Hamiltonian describing the effective one-electron atom interacting with the electromagnetic field, in the presence of the CAP, reads

$$H = H_{AT} + H_{EM} + H_I - i\eta W, \tag{6}$$

where

$$H_{AT} = -\frac{1}{2}\nabla^2 + V_{HS}(r), \tag{7}$$

$$H_{EM} = \sum_{k,\lambda} \omega a_{k,\lambda}^\dagger a_{k,\lambda}, \tag{8}$$

$$H_I = x \cdot \sum_{k,\lambda} i\sqrt{\frac{2\pi}{V}}\omega\{e_{k,\lambda} a_{k,\lambda} - e_{k,\lambda}^* a_{k,\lambda}^\dagger\}. \tag{9}$$

Here, H_{EM} represents the free electromagnetic field and H_I the interaction term in the electric-dipole approximation (in length gauge). The operator $a_{k,\lambda}^\dagger (a_{k,\lambda})$ creates (annihilates) a photon with wave vector k, polarization λ, and energy $\omega = k/\alpha$ (α is the fine-structure constant). We use the symbol x for the atomic dipole operator. V in Eq. (9) denotes the normalization volume of the electromagnetic field, and $e_{k,\lambda}$ indicates the polarization vector of mode k, λ.

Let N be the number of photons in the laser mode, so that the laser intensity is given by

$$I = \frac{N}{V}\frac{\omega}{\alpha}, \tag{10}$$

the intensity being measured in units of $I_0 = E_h/(t_0 a_0^2) = 6.436\,41 \times 10^{15}$ W/cm^2 (E_h is the Hartree energy, t_0 the atomic unit of time, and a_0 the Bohr radius). We can now combine the atomic eigenstates $\psi_{n,l,m} = [u_{n,l}(r)/r]Y_{l,m}(\vartheta,\varphi)$ with the Fock states of the laser mode, $|N-\mu\rangle$ ($\mu = 0, \pm 1, \pm 2, \ldots$), to form basis vectors $|\Phi_{n,l,m,\mu}\rangle = |\psi_{n,l,m}\rangle|N-\mu\rangle$. Assuming linear polarization, the matrix representation of the Hamiltonian H [Eq. (6)] in the basis $\{|\Phi_{n,l,m,\mu}\rangle\}$ is diagonal with respect to m. It also has a rather sparse structure with respect to n, l, and μ. The only nonzero matrix elements are

$$\langle\Phi_{n,l,m,\mu}|H_{AT} + H_{EM}|\Phi_{n,l,m,\mu}\rangle = \varepsilon_{n,l} - \mu\omega, \tag{11}$$

$$\langle\Phi_{n,l,m,\mu}|H_I|\Phi_{n',l',m,\mu+1}\rangle = \sqrt{2\pi\alpha I}\langle\psi_{n,l,m}|z|\psi_{n',l',m}\rangle, \tag{12}$$

$$\langle\Phi_{n,l,m,\mu+1}|H_I|\Phi_{n',l',m,\mu}\rangle = \sqrt{2\pi\alpha I}\langle\psi_{n,l,m}|z|\psi_{n',l',m}\rangle, \tag{13}$$

$$\langle\Phi_{n,l,m,\mu}|W|\Phi_{n',l,m,\mu}\rangle = \langle\psi_{n,l,m}|W|\psi_{n',l,m}\rangle. \tag{14}$$

The energy $N\omega$ of the unperturbed laser field has been subtracted from the right-hand side of Eq. (11); the relatively high intensity ($N \gg |\mu|$) has been exploited in the coupling matrix blocks [Eqs. (12) and (13)], and a unitary transformation has been applied that renders the matrix $H_{AT} + H_{EM} + H_I$ real symmetric. The complete matrix H is complex symmetric and of the Floquet type [76–81] (see, for example, Refs. [82–86] and references therein for other computational approaches to atomic strong-field physics). In our calculations, μ runs from $\mu_{min} = 0$ to μ_{max}, the minimum number of photons needed to photoionize (referred to as N.P. in Table I). Thus, since electron emission can only take place after the absorption of μ_{max} photons, it is sufficient to apply the CAP only to the (μ_{max})th diagonal block; i.e., $\langle\Phi_{n,l,m,\mu}|W|\Phi_{n',l,m,\mu}\rangle$ is set to 0 for $\mu \neq \mu_{max}$.
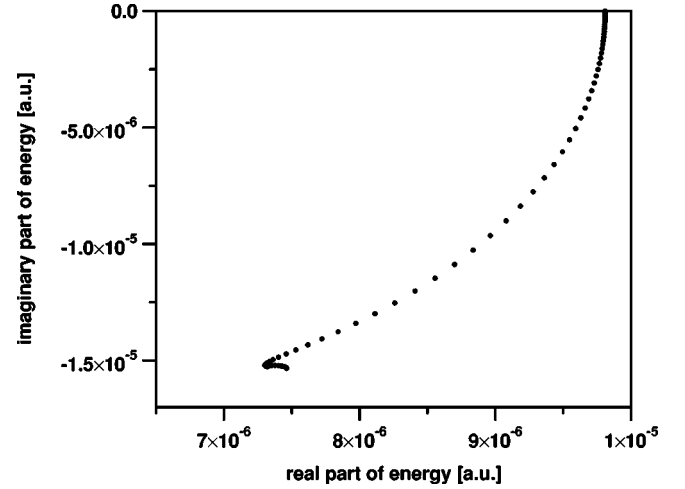

FIG. 2. The dots in this figure correspond to a specific eigenvalue of the family of complex symmetric matrices $H(\eta_n)$ [Eq. (6)], where $\eta_n = \delta(\kappa^n-1)/(\kappa-1)$ [$n=0,\ldots,99$; $\delta=3\times 10^{-9}$; $\kappa=1.1$]. In the absence of photons and absorbing potential, this eigenvalue equals the $5p$, $m=0$ level of atomic xenon (which defines the origin in the figure). Due to the interaction with 12.7-eV photons, this level is shifted as well as broadened. The point of stabilization of the η trajectory implies a dynamic Stark shift of 7.31×10^{-6} a.u. and an ionization rate of 3.05×10^{-5} a.u., at a radiation intensity of 1×10^{11} W/cm^2.

III. CALCULATIONS

As a test of our method, we determined the one-photon ionization cross section of neutral Xe at a photon energy of 12.7 eV. In this calculation, s, p, and d waves were included, and μ_{max} was set to 1. Let us first consider ionization of the $5p$, $m=0$ level. After assembling the corresponding real symmetric matrix $H_{AT} + H_{EM} + H_I$, those 120 eigenvectors of this matrix were computed that have the largest overlap with the initial-state vector $|\Phi_{5,1,0,0}\rangle$. The η-dependent complex symmetric eigenvalue problem of H [Eq. (6)] was then solved in the subspace of the previously calculated eigenvectors of the real part of H. The chosen subspace size of 120 provided converged results and, at the same time, allowed for extremely fast optimization of the parameter η [see Eq. (5) and the text following it].

The η trajectory of the resonance energy in the complex plane, for an intensity of 1×10^{11} W/cm^2, is shown in Fig. 2. On the basis of this graph, a dynamic Stark shift of 7.31×10^{-6} a.u. and an ionization rate of $\gamma_{5p,0}=3.05\times 10^{-5}$ a.u. are found. Proceeding in a similar fashion, the ionization rate of the $5p$, $m=\pm 1$ levels is calculated as $\gamma_{5p,\pm 1}=2.01\times 10^{-5}$ a.u. at 1×10^{11} W/cm^2, so that the m-averaged ionization rate

$$\bar{\gamma}_{5p} = (\gamma_{5p,-1} + \gamma_{5p,0} + \gamma_{5p,1})/3 \tag{15}$$

is 2.35×10^{-5} a.u. We then calculate the total ionization rate as

$$\Gamma_{5p} = \bar{\gamma}_{5p}(6-q), \tag{16}$$

where, for neutral Xe, $q=0$ (q is the atomic charge). This procedure is approximately valid also for $q>0$, since the

spin-orbit interaction ensures that the $6-q$ $5p$ electrons are uniformly distributed over $m=-1,0,+1$.

We have checked that Γ_{5p} is a linear function of the intensity, I, in the vicinity of 1×10^{11} W/cm^2. Thus, within the Herman-Skillman-based independent-particle model, the one-photon ionization cross section of neutral Xe, at a photon energy of 12.7 eV, is 119 Mb. This result, which differs from the experimental cross section [87] by a little more than a factor of 2, has been confirmed by us using the same independent-particle model, but treating the continuum problem with an R-matrix code [88] (see also Ref. [40]).

In order to test whether our CAP-Floquet program is also capable of describing multiphoton physics, we investigated the two-photon ionization cross section of neutral Xe at 6.42 eV. Experimentally, this is known to be about 4×10^{-50} s [89]. With atomic s through f waves and $\mu_{max}=2$, we calculated a cross section of 6.2×10^{-50} cm^4 s. Other calculations of this quantity, which are similarly accurate, are reported in Refs. [90–92].

We calculated the $(q+1)$-photon ionization cross section σ_{q+1} of Xe^{q+} at a photon energy of 12.7 eV (see Table I) following a strategy analogous to the one described above for neutral xenon:

$$\sigma_2(Xe^+) = 4.5 \times 10^{-49} \text{ cm}^4 \text{ s}, \qquad (17)$$

$$\sigma_3(Xe^{2+}) = 4.7 \times 10^{-84} \text{ cm}^6 \text{ s}^2, \qquad (18)$$

$$\sigma_4(Xe^{3+}) = 1.8 \times 10^{-115} \text{ cm}^8 \text{ s}^3, \qquad (19)$$

$$\sigma_5(Xe^{4+}) = 1.1 \times 10^{-148} \text{ cm}^{10} \text{ s}^4, \qquad (20)$$

$$\sigma_6(Xe^{5+}) = 2.4 \times 10^{-179} \text{ cm}^{12} \text{ s}^5. \qquad (21)$$

The spatial profile of the VUV-FEL beam in Hamburg, perpendicular to the beam axis, has a Gaussian shape [27]. Let (ρ,φ,z) denote cylindrical coordinates with respect to that axis. The intensity near the focus (at $z=0$) may then be written as

$$I(\rho,z,t) = \frac{4 \ln 2}{\pi \Delta^2(z)} \exp\left(-\frac{4 \ln 2}{\Delta^2(z)} \rho^2 \right) P(t), \qquad (22)$$

where

$$\Delta(z) = \Delta \sqrt{1 + (z/z_0)^2} \qquad (23)$$

is the z-dependent full width at half maximum of the Gaussian beam profile. In the experiment described in Ref. [26], $\Delta=20$ μm. The beam divergence was 17 mrad [27], from which we estimate that $z_0=1.2$ mm. The time-dependent pulse power is represented in Eq. (22) by $P(t)$.

Since we are interested in the *nonlinear* response of Xe ions to the vuv laser pulses, it is not permissible to use for $P(t)$ the pulse shape obtained after averaging over many pulses. The temporal shape of the individual FEL pulses has not been measured so far, but reliable simulations of the FEL performance exist [23,93], which are able to reproduce measured FEL parameters and which, in addition, provide information about temporal pulse shapes [94]. Ten representative, simulated pulses are shown in Fig. 3 [95]. We see that while
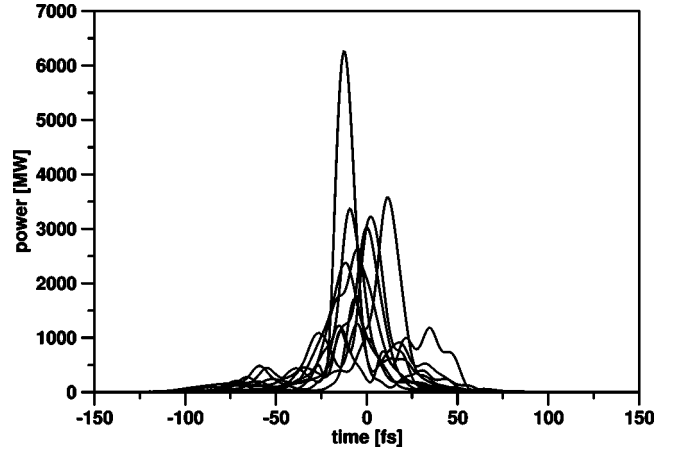

FIG. 3. The power in the DESY free-electron laser pulse is shown as a function of time. The vuv laser pulses supplied by the free-electron laser source at DESY, Hamburg, are ultrashort, with an average width of about 50 fs, and intense, with a pulse energy of order 10 μJ [23]. The pulses shown in this figure [95] have been calculated using an FEL simulation program [93,94].

the averaged pulse may appear approximately Gaussian (with a pulse width of about 50 fs), the individual pulses are not.

Including an attenuation factor of 0.2 [27], which takes into account the finite reflectivity of the mirrors used to focus the FEL beam into the xenon gas, we solve, for each of the pulses shown in Fig. 3, the rate equations

$$\dot{n}_0(\rho,z,t) = -\sigma_1 \frac{I(\rho,z,t)}{\omega} n_0(\rho,z,t),$$

$$\dot{n}_1(\rho,z,t) = \sigma_1 \frac{I(\rho,z,t)}{\omega} n_0(\rho,z,t) - \sigma_2 \left(\frac{I(\rho,z,t)}{\omega} \right)^2 n_1(\rho,z,t),$$

$$\dot{n}_2(\rho,z,t) = \sigma_2 \left(\frac{I(\rho,z,t)}{\omega} \right)^2 n_1(\rho,z,t) - \sigma_3 \left(\frac{I(\rho,z,t)}{\omega} \right)^3 n_2(\rho,z,t),$$

$$\vdots \qquad (24)$$

for the probabilities $n_q(\rho,z,t)$ of finding Xe^{q+} at time t and position (ρ,z) (φ arbitrary). (The thermal motion of the ions on a time scale of 100 fs may, of course, be neglected.) The initial conditions are $n_0(\rho,z,t \to -\infty)=1$ and $n_q(\rho,z,t \to -\infty)=0$ for $q>0$. Let κ stand for the gas density in the interaction region. Then the total number of Xe^{q+} generated by a given laser pulse reads

$$N_q = 2\pi\kappa \int_{z_{min}}^{z_{max}} dz \int_0^\infty d\rho \rho n_q(\rho,z,t \to +\infty). \qquad (25)$$

In the laser experiment at DESY, $\kappa=2.8 \times 10^{13}$ atoms/cm^3, $z_{min}=-1$ mm, and $z_{max}=+1$ mm [27].

We calculated N_q for each of the ten laser pulses in Fig. 3 and then determined the average number of Xe^{q+} generated per laser pulse, $\langle N_q \rangle$, which is depicted in Fig. 4. It is difficult to assess whether this result can already explain the measurements in Ref. [26]. According to the calculation, Xe$^+$ and
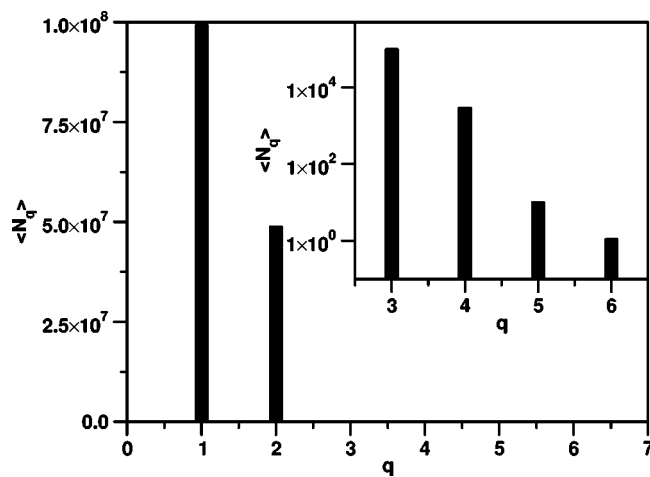
FIG. 4. The average number $\langle N_q \rangle$ of Xe^{q+} ions produced per VUV-FEL laser pulse, as calculated on the basis of the multiphoton ionization cross sections in Eqs. (17)–(21), the laser pulse properties [Eqs. (22) and (23) and Fig. 3], the rate equations (24), and the integral over the interaction volume in Eq. (25). Note the logarithmic scale along the ordinate of the inset.

Xe^{2+} dominate by far, which is consistent with the fact that the detector response to these two ions appeared to be saturated in the experiment [26]. The mass spectra in Ref. [26] have not been calibrated to account for the specific detector response to ions of different charge states [27], so they may not be linearly related to the actual ion production rate. Moreover, several of the experimental parameters we employed in our calculation are, in fact, not known very precisely. Among these are the gas density κ and the spatial beam width Δ [27]. It should be mentioned, in addition, that the FEL was not operating under optimal conditions when the data in Ref. [26] were taken [27]. Therefore, the laser pulses our calculation is based on (Fig. 3) are, on average, more intense than in the experiment.

The theoretical model we use also suffers from shortcomings. As mentioned earlier, multiplet splittings of the valence shell are not considered, which means the intermediate bound states influencing the multiphoton ionization cross sections may not be sufficiently accurate. The spectral width $\Delta \omega / \omega$ of the laser pulses of, on average, 1% [27]—which is broader than the Fourier limit of a 50-fs pulse by an order of magnitude—is not included in the present treatment. In the rate equations (24), excited-state populations and phase effects as well as nonsequential multiphoton processes are neglected. The latter, however, may be expected to be strongly suppressed in the vuv regime, as confirmed by the measurements in Ref. [26].

Before concluding, we would like to mention an interesting many-electron effect that leads to an enhancement of the multiphoton ionization rate in the xenon ions. In Xe^+, it requires 11.3 eV [96] to excite one of the two $5s$ electrons to the $5p$ shell. (Within the Herman-Skillman model we find 10.9 eV.) One can, therefore, envisage, as one of the paths leading to two-photon ionization of Xe^+, the excitation of a $5s$ electron by a first vuv photon and the subsequent excitation of one of the $5p$ electrons to a virtual state bound in the channel associated with the $5s$ hole, as illustrated in Fig. 5.
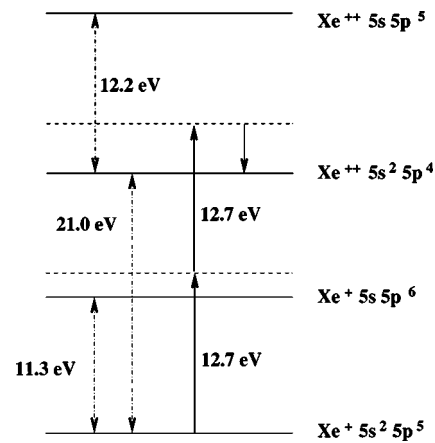

FIG. 5. Schematic depiction of energy levels associated with the excitation of xenon ions from the $5s$ subshell. For instance, Xe^+ can be photoionized via the absorption of two vuv photons by a $5p$ electron. A second ionization path, alluded to in this figure, involves a photon absorption that virtually excites a $5s$ electron to the $5p$ shell. Simultaneously, a $5p$ electron is excited to an autoionizing state associated with a Rydberg series converging to the $5s\,5p^5$ threshold of Xe^{2+}. Electron correlation then induces a transition from $5p$ to $5s$ accompanied by the emission of an electron.

Due to electron correlation, one of the remaining $5p$ electrons can fill the $5s$ hole, and the excited electron is ejected into the continuum. This is a kind of Auger decay of the inner-valence excited ion, resulting in the formation of Xe^{2+}. A similar scenario is conceivable for the more highly charged xenon ions.

The contribution of this to the multiphoton ionization cross section of Xe^{q+} can be crudely estimated as follows. We choose $|\Phi_{5,0,0,0}\rangle$ as initial-state vector in our Floquet code, but instead of utilizing a CAP, we simply assign an autoionization width Γ_{auto} (i.e., we add $-i\Gamma_{auto}/2$) to those diagonal elements in the (μ_{max})th diagonal block that satisfy $\varepsilon_{n,l} + \varepsilon_{5,1} - \varepsilon_{5,0} > 0$. This condition implies that the energy released in the $5p \rightarrow 5s$ transition is sufficient to transfer the electron with quantum numbers n and l into the continuum. A typical lifetime of an inner-shell hole is of the order of 10 fs (or shorter), so we set the autoionization width to 65 meV.

Let us call γ_{5s} the $5s$-mediated ionization rate determined in this way. The total $5s$-mediated ionization rate of Xe^{q+} is then, approximately,

$$\Gamma_{5s} = 2\gamma_{5s} \frac{q}{6}(7-q). \qquad (26)$$

The factor of 2 in this expression is needed since there are two $5s$ electrons in all Xe ions considered here. If we assume that the six $5p$ spin orbitals have equal probability of being occupied, then the probability that the $5p$, $m=0$ spin orbital with the right spin is unoccupied is $q/6$. After the virtual excitation of one of the $5s$ electrons, there are $7-q$ $5p$ electrons available for the absorption of the remaining $\mu_{max} - 1$ photons.
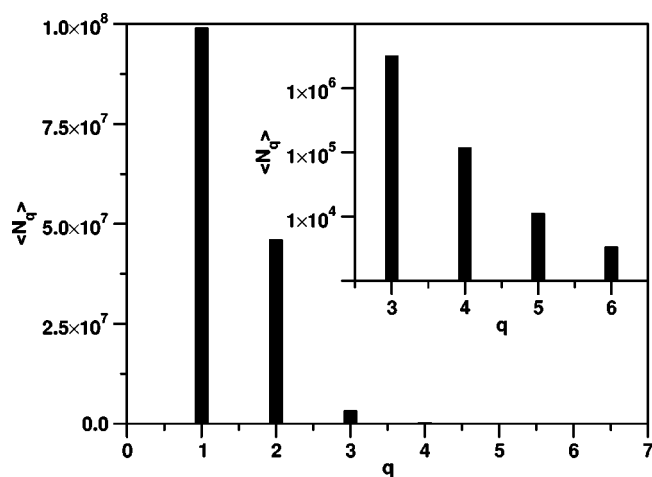
FIG. 6. The same as in Fig. 4, the only difference being the fact that the multiphoton ionization cross sections underlying the calculation were taken from Eqs. (27)–(31), not Eqs. (17)–(21). Here $\langle N_q \rangle$ is the average number of Xe^{q+} ions produced per VUV-FEL radiation pulse.

We add the cross sections obtained in this way to the respective cross sections in Eqs. (17)–(21), thereby neglecting interference effects. The results are

$$\sigma_2(Xe^+) = 4.6 \times 10^{-49} \text{ cm}^4 \text{ s}, \qquad (27)$$

$$\sigma_3(Xe^{2+}) = 2.0 \times 10^{-82} \text{ cm}^6 \text{ s}^2, \qquad (28)$$

$$\sigma_4(Xe^{3+}) = 3.3 \times 10^{-115} \text{ cm}^8 \text{ s}^3, \qquad (29)$$

$$\sigma_5(Xe^{4+}) = 3.7 \times 10^{-147} \text{ cm}^{10} \text{ s}^4, \qquad (30)$$

$$\sigma_6(Xe^{5+}) = 6.4 \times 10^{-179} \text{ cm}^{12} \text{ s}^5. \qquad (31)$$

The quantities most significantly affected by the $5s$-mediated ionization mechanism are the three-photon ionization cross section of Xe^{2+} and the five-photon ionization cross section of Xe^{4+}.

The ionic charge distribution computed using the multiphoton ionization cross sections in Eqs. (27)–(31) is displayed in Fig. 6. Now the production of Xe^{3+} is clearly visible even on a linear scale: About 3×10^6 triply charged xenon ions are produced per laser pulse. The number of Xe^{6+} ions per laser pulse is more than 3000, which is also not particularly small.

IV. CONCLUSION

We have investigated in this paper multiphoton ionization of atomic xenon and its ions at a photon energy of 12.7 eV, a radiation intensity of order 10^{13} W/cm^2, and a pulse duration of about 50 fs. A recent experiment employing the VUV-FEL at DESY has demonstrated, under these laser conditions, the generation of xenon charge states of up to 6+ [26]. In the infrared, even a pulse that is three orders of magnitude longer (with about the same intensity), produces charge states no higher than Xe^{4+} [33].

Using an effective one-particle model, in combination with the Floquet concept and a complex absorbing potential, we have calculated vuv multiphoton ionization cross sections that refer to the absorption, by a $5p$ electron, of as many photons as are needed to ionize it. We have also estimated the influence of $5s$ excitation on the ionization cross sections and found that it may be significant. Although we grant that the model we applied is not ideal for describing many-electron phenomena (a better many-body calculation would be desirable), the result of our estimate indicates that at vuv photon energies multiphoton ionization is driven, at least partly, by electronic many-body physics. Focusing on the behavior of a single active electron does not appear to be sufficient.

Taking a rate-equation approach and utilizing simulated FEL pulses [95], we determined the average number of Xe^{q+} ions produced per vuv laser pulse. This step depends heavily on a number of important experimental parameters [27]. In our calculation, thousands of Xe^{6+} ions are found to be generated per pulse and a correspondingly higher number for the lower charge states. Hence, the experimental observation of multiple ionization of xenon, Ref. [26], appears compatible with the nonlinear absorption of several photons. We conclude that multiphoton physics is indeed relevant for some processes driven by the intense vuv beam of the free-electron laser in Hamburg. For more quantitative comparisons, it will be desirable for future experiments to obtain a calibrated ionic charge distribution, as well as more detailed information about the FEL pulse properties.

[1] L. V. Keldysh, Zh. Eksp. Teor. Fiz. **47**, 1945 (1964) [Sov. Phys. JETP **20**, 1307 (1965)].

[2] F. H. M. Faisal, J. Phys. B **6**, L89 (1973).

[3] H. R. Reiss, Phys. Rev. A **22**, 1786 (1980).

[4] M. V. Ammosov, N. B. Delone, and V. P. Krainov, Zh. Eksp.

Teor. Fiz. **91**, 2008 (1986) [Sov. Phys. JETP **64**, 1191 (1986)].

[5] P. B. Corkum, Phys. Rev. Lett. **71**, 1994 (1993).

[6] *Multiphoton Processes*, edited by J. H. Eberly and P. Lambropoulos (Wiley, New York, 1978).

[7] F. H. M. Faisal, *Theory of Multiphoton Processes* (Plenum

Press, New York, 1987).

[8] *Multiphoton Processes*, edited by S. J. Smith and P. L. Knight (Cambridge University Press, Cambridge, England, 1988).

[9] M. H. Mittleman, *Introduction to the Theory of Laser-Atom Interactions* (Plenum Press, New York, 1993).

[10] E. L. Saldin, E. A. Schneidmiller, and M. V. Yurkov, *The Physics of Free Electron Lasers* (Springer-Verlag, Berlin, 1999).

[11] *Proceedings of the 24th International Free Electron Laser Conference and the 9th Users Workshop, Argonne, IL*, 2002, edited by K.-J. Kim, S. V. Milton, and E. Gluskin [Nucl. Instrum. Methods Phys. Res. A **507**, 1 (2003)].

[12] M. Brewczyk and K. Rzazewski, J. Phys. B **32**, L1 (1999).

[13] M. Gajda, J. Krzywinski, L. Plucinski, and B. Piraux, J. Phys. B **33**, 1271 (2000).

[14] S. A. Novikov and A. N. Hopersky, J. Phys. B **33**, 2287 (2000).

[15] J. Bauer, L. Plucinski, B. Piraux, R. Potvliege, M. Gajda, and J. Krzywinski, J. Phys. B **34**, 2245 (2001).

[16] K. Ishikawa and K. Midorikawa, Phys. Rev. A **65**, 043405 (2002).

[17] S. A. Novikov and A. N. Hopersky, J. Phys. B **35**, L339 (2002).

[18] U. Saalmann and J.-M. Rost, Phys. Rev. Lett. **89**, 143401 (2002).

[19] L. A. A. Nikolopoulos, T. Nakajima, and P. Lambropoulos, Phys. Rev. Lett. **90**, 043003 (2003).

[20] I. F. Barna and J.-M. Rost, Eur. Phys. J. D **27**, 287 (2003).

[21] R. Santra and L. S. Cederbaum, Phys. Rev. Lett. **90**, 153401 (2003).

[22] J. Andruszkow *et al.*, Phys. Rev. Lett. **85**, 3825 (2000).

[23] V. Ayvazyan *et al.*, Phys. Rev. Lett. **88**, 104802 (2002).

[24] H. Wabnitz, L. Bittner, A. R. B. de Castro, R. Döhrmann, P. Gürtler, T. Laarmann, W. Laasch, J. Schulz, A. Swiderski, K. von Haeften, T. Möller, B. Faatz, A. Fateev, J. Feldhaus, C. Gerth, U. Hahn, E. Saldin, E. Schneidmiller, K. Sytchev, K. Tiedtke, R. Treusch, and M. Yurkov, Nature (London) **420**, 482 (2002).

[25] R. Santra and C. H. Greene, Phys. Rev. Lett. **91**, 233401 (2003).

[26] H. Wabnitz, A. R. B. de Castro, P. Gürtler, T. Laarmann, W. Laasch, J. Schulz, and T. Möller (unpublished).

[27] T. Möller and H. Wabnitz (private communication).

[28] S. Geltman, Phys. Rev. Lett. **54**, 1909 (1985).

[29] J. Zakrzewski, J. Phys. B **19**, L315 (1986).

[30] S. Geltman and J. Zakrzewski, J. Phys. B **21**, 47 (1988).

[31] A. L'Huillier, L. A. Lompre, G. Mainfray, and C. Manus, Phys. Rev. Lett. **48**, 1814 (1982).

[32] T. S. Luk, H. Pummer, K. Boyer, M. Shahidi, H. Egger, and C. K. Rhodes, Phys. Rev. Lett. **51**, 110 (1983).

[33] A. L'Huillier, L. A. Lompre, G. Mainfray, and C. Manus, J. Phys. B **16**, 1363 (1983).

[34] A. L'Huillier, L. A. Lompre, G. Mainfray, and C. Manus, Phys. Rev. A **27**, 2503 (1983).

[35] F. Yergeau, S. L. Chin, and P. Lavigne, J. Phys. B **20**, 723 (1987).

[36] A. Szabo and N. S. Ostlund, *Modern Quantum Chemistry* (Dover, Mineola, NY, 1996).

[37] J. C. Slater, Phys. Rev. **81**, 385 (1951).

[38] J. C. Slater and K. H. Johnson, Phys. Rev. B **5**, 844 (1972).

[39] F. Herman and S. Skillman, *Atomic Structure Calculations* (Prentice-Hall, Englewood Cliffs, NJ, 1963).

[40] S. T. Manson and J. W. Cooper, Phys. Rev. **165**, 126 (1968).

[41] F. Brandi, I. Velchev, W. Hogervorst, and W. Ubachs, Phys. Rev. A **64**, 032505 (2001).

[42] J. E. Hansen and W. Persson, Phys. Scr. **36**, 602 (1987).

[43] D. Mathur and C. Badrinathan, Phys. Rev. A **35**, 1033 (1987).

[44] D. C. Gregory, P. F. Dittner, and D. H. Crandall, Phys. Rev. A **27**, 724 (1983).

[45] F. H. Dorman, J. D. Morrison, and A. J. C. Nicholson, J. Chem. Phys. **31**, 1335 (1959).

[46] F. A. Stuber, J. Chem. Phys. **42**, 2639 (1965).

[47] J. A. Syage, Phys. Rev. A **46**, 5666 (1992).

[48] H.-J. Werner and P. J. Knowles, J. Chem. Phys. **82**, 5053 (1985).

[49] P. J. Knowles and H.-J. Werner, Chem. Phys. Lett. **115**, 259 (1985).

[50] L. A. LaJohn, P. A. Christiansen, R. B. Ross, T. Atashroo, and W. C. Ermler, J. Chem. Phys. **87**, 2812 (1987).

[51] K. J. Bathe, *Finite Element Procedures in Engineering Analysis* (Prentice Hall, Englewood Cliffs, NJ, 1976).

[52] K. J. Bathe and E. Wilson, *Numerical Methods in Finite Element Analysis* (Prentice Hall, Englewood Cliffs, NJ, 1976).

[53] M. Braun, W. Schweizer, and H. Herold, Phys. Rev. A **48**, 1916 (1993).

[54] J. Ackermann and J. Shertzer, Phys. Rev. A **54**, 365 (1996).

[55] T. N. Rescigno, M. Baertschy, D. Byrum, and C. W. McCurdy, Phys. Rev. A **55**, 4253 (1997).

[56] K. W. Meyer, C. H. Greene, and B. D. Esry, Phys. Rev. Lett. **78**, 4902 (1997).

[57] R. Santra, K. V. Christ, and C. H. Greene, Phys. Rev. A **69**, 042510 (2004).

[58] A. Goldberg and B. W. Shore, J. Phys. B **11**, 3339 (1978).

[59] G. Jolicard and E. J. Austin, Chem. Phys. Lett. **121**, 106 (1985).

[60] G. Jolicard and E. J. Austin, Chem. Phys. **103**, 295 (1986).

[61] D. Neuhauser and M. Baer, J. Chem. Phys. **90**, 4351 (1989).

[62] U. V. Riss and H.-D. Meyer, J. Phys. B **26**, 4503 (1993).

[63] U. V. Riss and H.-D. Meyer, J. Phys. B **28**, 1475 (1995).

[64] N. Moiseyev, J. Phys. B **31**, 1431 (1998).

[65] U. V. Riss and H.-D. Meyer, J. Phys. B **31**, 2279 (1998).

[66] J. P. Palao, J. G. Muga, and R. Sala, Phys. Rev. Lett. **80**, 5469 (1998).

[67] J. P. Palao and J. G. Muga, J. Phys. Chem. A **102**, 9464 (1998).

[68] H. O. Karlsson, J. Chem. Phys. **109**, 9366 (1998).

[69] T. Sommerfeld, U. V. Riss, H.-D. Meyer, L. S. Cederbaum, B. Engels, and H. U. Suter, J. Phys. B **31**, 4107 (1998).

[70] R. Santra and L. S. Cederbaum, J. Chem. Phys. **115**, 6853 (2001).

[71] R. Santra and L. S. Cederbaum, Phys. Rep. **368**, 1 (2002).

[72] D. E. Manolopoulos, J. Chem. Phys. **117**, 9552 (2002).

[73] B. Poirier and T. Carrington, Jr., J. Chem. Phys. **118**, 17 (2003).

[74] B. Poirier and T. Carrington, Jr., J. Chem. Phys. **119**, 77 (2003).

[75] D. P. Craig and T. Thirunamachandran, *Molecular Quantum Electrodynamics* (Dover, Mineola, NY, 1998).

[76] J. H. Shirley, Phys. Rev. **138**, B979 (1965).

[77] S.-I Chu and W. P. Reinhardt, Phys. Rev. Lett. **39**, 1195

(1977).

[78] S.-I Chu and J. Cooper, Phys. Rev. A **32**, 2769 (1985).

[79] P. G. Burke, P. Francken, and C. J. Joachain, J. Phys. B **24**, 751 (1991).

[80] M. Dörr, M. Terao-Dunseath, J. Purvis, C. J. Noble, P. G. Burke, and C. J. Joachain, J. Phys. B **25**, 2809 (1992).

[81] S.-I Chu and D. A. Telnov, Phys. Rep. **390**, 1 (2004).

[82] K. C. Kulander, Phys. Rev. A **35**, R445 (1987).

[83] K. C. Kulander, Phys. Rev. A **38**, 778 (1988).

[84] E. Huens, B. Piraux, A. Bugacov, and M. Gajda, Phys. Rev. A **55**, 2132 (1997).

[85] K. T. Taylor and D. Dundas, Philos. Trans. R. Soc. London, Ser. A **357**, 1331 (1999).

[86] G. Lagmago Kamta and A. F. Starace, Phys. Rev. A **65**, 053418 (2002).

[87] J. A. R. Samson, in *Advances in Atomic and Molecular Physics*, edited by D. R. Bates and I. Estermann (Academic Press, New York, 1966), Vol. 2.

[88] M. Aymar, C. H. Greene, and E. Luc-Koenig, Rev. Mod. Phys. **68**, 1015 (1996).

[89] A. W. McCown, M. N. Ediger, and J. G. Eden, Phys. Rev. A **26**, 3318 (1982).

[90] E. J. McGuire, Phys. Rev. A **24**, 835 (1981).

[91] P. Gangopadhyay, X. Tang, P. Lambropoulos, and R. Shakeshaft, Phys. Rev. A **34**, 2998 (1986).

[92] A. L'Huillier and G. Wendin, J. Phys. B **20**, L37 (1987).

[93] E. L. Saldin, E. A. Schneidmiller, and M. V. Yurkov, Nucl. Instrum. Methods Phys. Res. A **429**, 233 (1999).

[94] M. Dohlus, K. Flöttmann, O. S. Kozlov, T. Limberg, Ph. Piot, E. L. Saldin, E. A. Schneidmiller, and M. V. Yurkov, Nucl. Instrum. Methods Phys. Res. A **530**, 217 (2004).

[95] M. V. Yurkov (private communication).

[96] C. E. Moore, *Atomic Energy Levels*, Natl. Stand. Ref. Data Ser. 35 (U.S. GPO, Washington, D.C., 1971).